



# Robust Diabetic Retinopathy Detection and Grading using Neutrosophic Topological Vector Space on Fundus Imaging

Mohammed Abdullah Al-Hagery<sup>1,\*</sup>, Abdalla I. Abdalla Musa<sup>1</sup>

<sup>1</sup>Department of Computer Science, College of Computer, Qassim University, Buraydah, Saudi Arabia  
Emails: hajry@qu.edu.sa; ab.musa@qu.edu.sa

## Abstract

Diabetic retinopathy (DR) is an eye disorder triggered by diabetes that might result in loss of sight. Earlier diagnosis of DR is critical since it might cause loss of sight. Manual diagnoses of DR severity by ophthalmologists are time-consuming and challenging. As a result, there has been considerable attention on designing an automatic technique for DR detection using fundus photographs. In medical science, prognosis and diagnosis are the most challenging tasks due to the presence of fuzziness in medical images and the restricted subjectivity of the experts. Neutrosophic Set (NS) in medical image analysis provides an understanding of the NS concepts, together with knowledge of how to collect, handle, interpret, and analyze clinical images using NS techniques. The neutrosophic set (NS), which is a generality of fuzzy set, provides the overcoming prospect of the restriction of fuzzy-based models for the analysis of medical images. This manuscript develops a Robust Diabetic Retinopathy Detection and Grading using Neutrosophic Topological Vector Space (DRDG-NSTVS) technique on fundus images. The DRDG-NSTVS technique begins with Median Filter (MF) noise removal to optimize the clarity of fundus photographs by successfully eliminating noises. Later, the InceptionV3 is used to perform feature extraction for identifying complicated features and patterns related to DR. The parameter tuning is performed by the moth flame optimization (MFO) technique to ensure superior performance of the model. The final diagnoses and classification of DR are accomplished utilizing the NSTVS classifiers that easily perform the uncertainties inherent in medicinal statistics. The simulation was conducted on a benchmark dataset to examine the proposed model performance. This combined method gives a greatly reliable and accurate solution for the earlier diagnosis and detection of DR

**Keywords:** Artificial Intelligence; Learning System; Machine learning; Diabetic Retinopathy; Neutrosophic Sets

## 1. Introduction

With the inspiring overview of the fuzzy set (FS), the research of uncertainty observed a major flow in technical exploration [1]. This initial thought paved the method for many theoretic additions and generalizations, driving its application through numerous areas [2]. These additions contain intuitionistic FS (IFS), cubic set, Pythagorean FS (PFS), interval-valued FS (IVFS), interval-valued PFS (IVPFS), and cubic PFS (CPFS), among others [3]. Particularly, the overview of the soft set (SS) by Molodtsov transformed the parameterization of sub-sets in any universal set [4]. Also, Smarandache explained the theory of hypersoft set (HSS), highlighting its importance over conventional SS [5]. While FS and its numerous additions are very beneficial numerical techniques to overwhelm uncertainty, which is beneficial to utilize these models on the uncertainty issue [6]. Owing to the deficiency of a parameterization tool, Molodtsov projected the SS model [7].

Diabetic retinopathy (DR) is a vision-threatening medicinal disease in which the retina of diabetic patients gets injured for a huge amount [8]. It is a secondary disorder that begins in people, who already suffer from Diabetes Mellitus [9]. It is one of the most foremost and frequent cases of blindness among adults and children who have been suffering from diabetes for a very long time [10]. The sturdy causes and links behind DR are extended periods of diabetes, glycaemic control, and poor blood pressure [11]. Presently, deep learning (DL) is normally applied for image identification in the field of computer vision (CV). Mainly, the most effective method in the area of CV is Convolutional Neural Networks (CNNs) over Transfer Learning (TL) [12]. A Where, a CNN contains a pooling layer, a convolution (Conv) layer, and a fully connected (FC) layer. When inventing the Conv layer, we want to

study parameters like manifold filters, the dimension of the Conv kernel, and then the sliding window [13]. To diminish the network parameter, a pooling layer is inserted among the Conv layers to make simpler the method. Lastly, the FC layer performs as a classifier in complete CNN [14]. The feature space gets the original data from the Conv and pooling layers and transmits the learned feature over FC layers into the space of the label. Then, the features are employed for exact tasks of image processing like recognition and segmentation [15].

This manuscript develops a Robust Diabetic Retinopathy Detection and Grading using Neutrosophic Topological Vector Space (DRDG-NSTVS) technique on fundus images. The DRDG-NSTVS technique begins with Median Filter (MF) noise removal to optimize the clarity of fundus photographs by successfully eliminating noises. Later, the InceptionV3 is used to perform feature extraction for identifying complicated features and patterns related to DR. The parameter tuning is performed by the moth flame optimization (MFO) technique to ensure superior performance of the model. The final diagnoses and classification of DR are accomplished using the NSTVS classifiers that easily perform the uncertainties inherent in medicinal statistics. The simulation was conducted on a benchmark dataset to examine the proposed model performance.

## **2. Related Works**

Hai et al. [16] presented the Diabetic Retinopathy Grading Convolutional Neural Network (DRGCNN) technique. This method utilized a more balanced technique by allotting an identical channel number to feature maps depicting several DRs. Moreover, the approach presents a CAM-EfficientNetV2-M encoding, which is specifically designed to encode input retinal fundus imageries for generating feature vectors. Furthermore, to yield benefit of the binocular relationship, the technique inputs fundus retinal imageries from both patient eyes into the network for feature fusion at the time of the training stage. In [17], DL techniques are employed for classifying the fundus images. Before the training, numerous image pre-processing models are utilized to remove the noise and objects from the imageries in order to enhance the excellence. A shallow CNN is presented by employing 3 blocks of max pool and convolution layers and is also implemented for determining the optimum data augmentation model.

Romero-Oraá et al. [18] present an end-to-end DL methodology for automatically grading the DR. The proposed model is dependent on a new attention mechanism that concentrates distinctly on the bright and dark retina structures by accomplishing a prior image decay. The technique also comprises an image quality evaluation phase and DL-based methods, namely transfer learning, data augmentation, and fine-tuning. Yamin et al. [19] proposes a DL Enabled Large Scale Healthcare Decision Making for DR (DLLSHDM-DR) technique. In the presented model, image pre-processing is achieved to enhance the fundus imagery quality. Additionally, the DLLSHDM-DR model utilizes HybridNet to produce an ensemble of feature vectors. Furthermore, the approach employs Emperor Penguin Optimizer (EPO) and DRNN models for classification. The EPO method helps in the optimum alteration of the hyperparameter associated with the DRNN technique.

Shamrat et al. [20] aim to automate the DR classifying procedure into several phases by employing CNN techniques. This approach utilized the accomplishment of 15 pre-trained methods with the new introduced diabetic retinopathy network (DRNet13) method. This methodology also intended to discriminate the effectual technique for precise DR performance depending on fundus imageries from 5 DR classes. The model pre-processed the image implementing a median filter (MF) for Gamma correction and noise elimination for image enhancement. Chavan and Choubey [21] propose a Frame-wise Severity Scale Classification Model (FSSCM) model employing TL and EfficientNet-B3 methods. The ResNet 101 approaches such as FT-RN 101 and TL-EN3 models are employed for fine-tuning. The Chan-Vese technique is employed for segmentation after pre-processing and augmentation procedures. The presented technique also employed the TL-EN3 method for capturing higher-resolution designs with greater accuracy and incorporates FT-RN 101 methods.

## **3. The Proposed Methodology**

In this manuscript, we have developed a robust DRDG-NSTVS technique on fundus images. It encompasses four different stages involved MF-based preprocessing, feature extraction using InceptionV3, parameter selection using MFO, and NSTVS-based DR classification stages are demonstrated in Fig. 1.

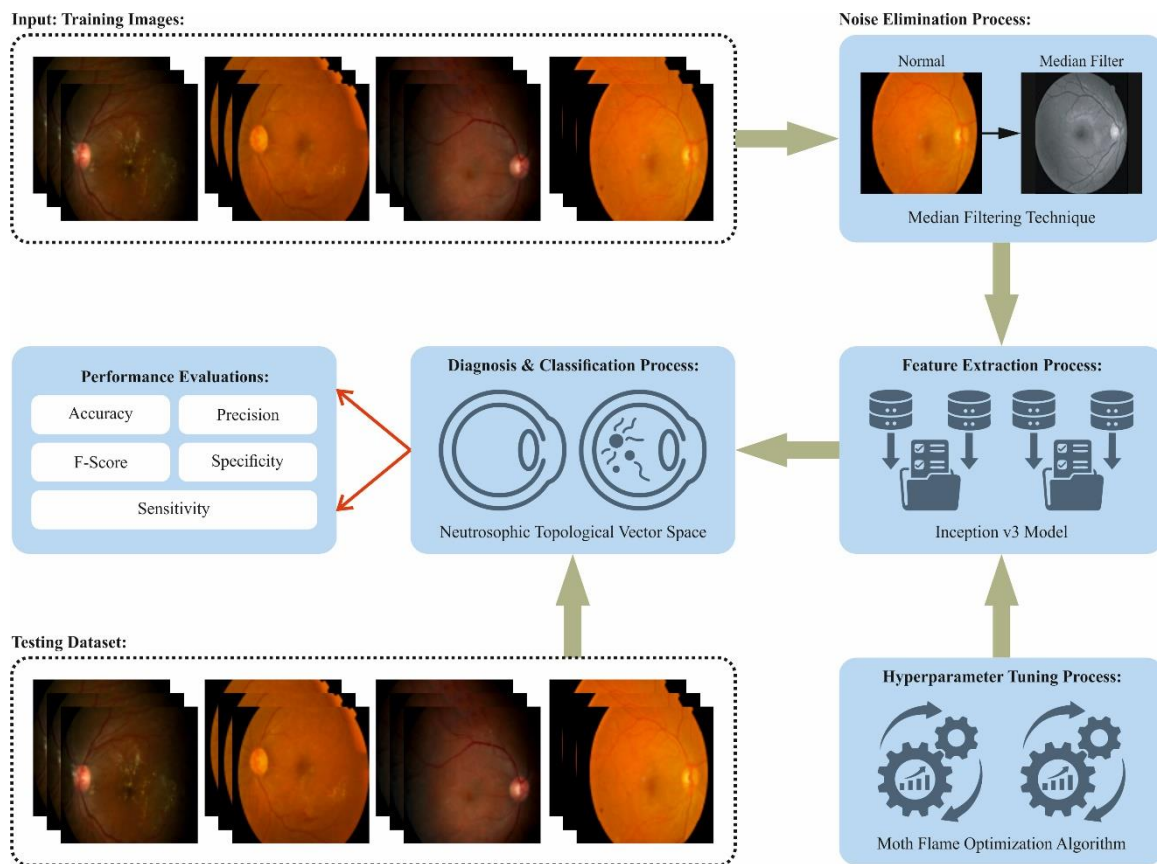


Figure 1: Overall process of DRDG-NSTVS technique

### A. Stage I: MF Pre-processing

Initially, the DRDG-NSTVS technique takes place MF noise removal to optimize the clarity of fundus photographs by successfully eliminating noises. MF is a general image processing model utilized for noise smoothing and reduction [22]. In this technique, a sliding window is used for every pixel of the image, and the pixel values within the window are kept. The central value (median) of this fixed set is then allotted to the pixel below consideration. This procedure efficiently removes outliers or random noise in the image, as the median value is less sensitive to great values than other statistical measures like the mean. One of the foremost benefits of MF is its capability to uphold edges and fine details in an image while efficiently decreasing salt-and-pepper noise or impulse noise. This is mainly beneficial in applications where upholding image quality and clarity is vital. In addition, MF is computationally effective and direct to implement, making it a general choice in real image processing uses. However, it may not be as effective in decreasing Gaussian or uniform noise when equated to other filtering approaches exactly intended for such noise kinds.

### B. Stage II: Inceptionv3 Architecture

Next, InceptionV3 is used to perform feature extraction for identifying complicated features and patterns related to DR. The input to the InceptionV3 system is an image of  $299 \times 299 \times 3$  [23]. The network covers 3 dissimilar kinds of inception modules ( $35 \times 35 / 17 \times 17 / 8 \times 8$ ) and dual Grid Size Reduction units. The Grid Size Reduction module resolves the issue of feature bottleneck and computational overload and lastly attains image identification detection by utilizing the function of softmax. The most significant feature of the InceptionV3 is splitting the higher 2D convolutional (Conv) kernel into dual small one-bit Conv kernels, e.g., decaying a  $5 \times 5$  Conv kernel into two  $3 \times 3$  Conv kernels, this enhances the network performance and raising the computation speed while decreasing the computation cost. Moreover, the network decays symmetric into asymmetric convolution kernels, by dividing the  $3 \times 3$  Conv kernels into  $1 \times 3$  and  $3 \times 1$  Conv kernels. The deconvolution kernel technique keeps a huge amount of parameters and speeds up the calculation while decreasing over-fitting. And, to resolve the issue of feature representation bottleneck and extreme calculation, dual Grid Size Reduction modules have been inserted among every 3 Inception Module to diminish the dimension of the feature map by employing a similar dual branch structure (pooling and convolution). The fully connected (FC) layer has been nominated for processing, which attains a higher level of feature integration. So, we select the FC layer as the data source for the extraction of the feature. Fig. 2 depicts the infrastructure of InceptionV3.

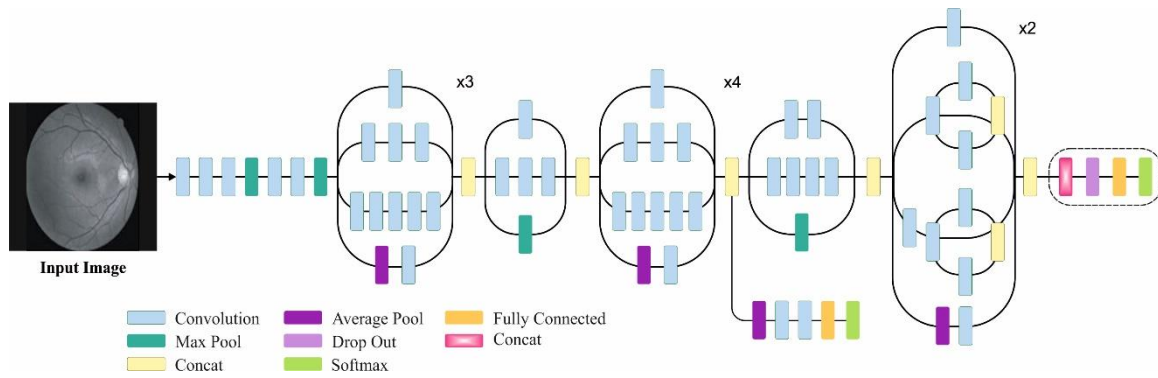


Figure 2: InceptionV3 architecture

**C. Stage III: MFO Parameter Selection**

At this stage, the parameter tuning is performed by the MFO technique to ensure superior performance of the model. MFO is a new metaheuristic approach inspired by the adjacent navigation method of moths [24]. It has a distinctive way to navigate during the night-time. By employing a transverse orientation device, it depends on moonlight to fly in a straight line that retains a fixed angle. The authors show that the moth location is a adaptable in resolving the optimizer problems in MFO technique, and the fame is the current optimum location. Moths get closer to the global best location by modifying the position vector. The matrix  $M$  represents the moth's location as follows:

$$M = \begin{bmatrix} m_{1,1} & m_{1,2} & \dots & m_{1,d} \\ m_{2,1} & m_{2,2} & \dots & m_{2,d} \\ \vdots & \vdots & & \vdots \\ m_{n,1} & m_{n,2} & \dots & m_{n,d} \end{bmatrix}, \tag{1}$$

In Eq. (1),  $n$  and  $d$  denotes the amount of moths and the size of control variables correspondingly. The fitness value is stored in matrix  $OM$  which represented below:

$$OM = \begin{bmatrix} OM_1 \\ OM_2 \\ \vdots \\ OM_n \end{bmatrix}, \tag{2}$$

Now  $n$  denotes the number of moths.

The MFO technique needs moth to upgrade the location utilizing the exclusive fame equivalent to it that efficiently evades local optima. Thus, the moth population is constant.  $F$  represents the position of fame.

$$F = \begin{bmatrix} F_{1,1} & F_{1,2} & \dots & F_{1,d} \\ F_{2,1} & F_{2,2} & \dots & F_{2,d} \\ \vdots & \vdots & & \vdots \\ F_{n,1} & F_{n,2} & \dots & F_{n,d} \end{bmatrix}, \tag{3}$$

The matrix  $OF$  keeps the fitness value of fame:

$$OP = \begin{bmatrix} OF_1 \\ OF_2 \\ \vdots \\ OF_n \end{bmatrix}, \tag{4}$$

Where  $n$  denotes the number of moths.

The search space is inhabited by moths, and every individual hunts for fame by updating and tagging it as the best solution. MFO represents the globally best ternary:

$$MFO = (I, P, T). \tag{5}$$

The function  $I$  produces a moth population and the fitness value.

$$I: \phi \rightarrow \{M, OM\}. \tag{6}$$

$P$  indicates the principal function, which moves the moth over the search ranges. Matrix  $M$  is known by  $P$ , and returns the upgraded value.

$$P: M \rightarrow M. \quad (7)$$

The function  $T$  returns true if the terminating condition is met; or else, it returns false.

$$T: M \rightarrow \{true, false\}. \quad (8)$$

After initializing function  $I$ , Function  $P$  changes the moth's location within the search range. Until the function  $T$  returns the true, the iteration is performed.

The selection of fitness is the significant factor inducing the performance of the MFO model. The hyperparameter range method contains the solution encode technique to gauge the efficiency of the candidate solution. In this work, the MFO system reflects accuracy as the foremost standard to project the fitness function (FF), which expressed below.

$$Fitness = \max(P) \quad (9)$$

$$P = \frac{TP}{TP + FP} \quad (10)$$

Here,  $TP$  signifies the value of true positive and  $FP$  represents the value of false positive.

#### D. Stage IV: NSTVS Architecture

The final diagnoses and classification of DR are accomplished using the NSTVS classifiers that easily perform the uncertainties inherent in medicinal statistics. NTVS is an addition of classical topological vector space to accommodate a neutrosophic set (NS), capturing the concept of unknown information, indeterminacy, and ambiguity [25]. This explores the intersection of topological vector spaces and NS theory, which offers a thorough knowledge of their applications and properties. We investigate the mathematical foundation, that defines an NTVS and explore its unique features. The incorporation of neutrosophic logic into these contexts provides an effective mechanism for managing imprecise and uncertain data, which makes NTVS an essential basis for many real-time applications.

**Definition 3.1:** Consider  $N$  and  $M$  as the NS and  $X$  and  $Y$  as two non-empty sets. The neutrosophic subset  $F$  of  $X \times Y$  is a neutrosophic proper function (NPF) from the NS ( $N$ ) to the ( $M$ ) if

$$(i) F(x, y) \leq N(x) \cap M \text{ for } (x, y) \in X \times Y.$$

$$(ii) \text{ For } \chi \in X_t \text{ there is a unique } y_0 \in Y \text{ so that } F(x, y_0) = N(x) \text{ and } F(x, y) = (0, 1) \text{ if } y \neq y_0.$$

Hence  $F: N \rightarrow M$  where  $F$  denotes an NPF from  $N \in N^X$  into  $M \in N^Y$ , where  $N^X$  and  $N^Y$  are the group of  $X$  and  $Y$  neutrosophic subsets, correspondingly.

**Definition 3.2:** A NS  $N = (x, I_N, \vartheta_N)$  of vector space  $X$  over  $K$  is an NVS over  $X$  if

$$N + N + N \subseteq N$$

$\alpha N \subseteq N$ , for scalar  $\alpha$ .

**Definition 3.3:** Assume  $N(X)$  as an NVS over  $K$  (complex or real) and a  $\tau$  topology is determined on it. The set  $N(X)$  is known as an NTVS if the map is

$$N^\oplus: (V \times V, \tau \times \tau) \rightarrow (V, \tau)$$

$$N^\ominus: (V \times V, \tau \times \tau) \rightarrow (V, \tau)$$

The couple  $(N(X), \tau)$  is represented by NTVS. Furthermore, the components of  $\tau$  are known as Neutrosophic open sets.

**Definition 3.4:** NPF: Consider  $X$  as a vector space over  $K$  with  $\theta$  as a null vector. Assume  $V$  as an NVS over  $X$ ,  $a \in X$  and  $k \in \mathbb{R}$  are fixed.

$$N^\oplus: V \times V \times V \rightarrow V \text{ by } N^\oplus((x, y, z), t) = \begin{cases} (V \times V \times V)(x, y, z) & \text{if } x + y + z = t \\ (0_t, 1) & \text{if } x + y + z \neq t \end{cases}$$

$$N^\odot: K \times V \rightarrow V \text{ by } N^\odot((k, x), r) = \begin{cases} K \times (V)(k, x) & \text{if } kx = y, k \neq 0 \\ \sup_{x \in X} V(x) & \text{if } kx = y, k = 0 \\ (0_t 1) & \text{if } kx \neq y \end{cases}$$

$$N^a: V \rightarrow V \text{ by } N^a((k, x), r) = \begin{cases} V(x) & \text{if } y = k_0x, k \neq 0 \\ (0,1) & \text{if } kx \neq y \end{cases}$$

$$N^{k_0}: V \rightarrow V \text{ by } N^{k_0}((x_t y)) = \begin{cases} K \times V(k, x) & \text{if } y = k_0x, k_0 \neq 0 \\ \sup_{x \in X} V(x) & \text{if } k_0x = y, k_0 = 0 \\ (0,1) & \text{if } k_0x \neq y \end{cases}$$

$$N_V^{L_{k,m,n}}((x, y, z), t) = \begin{cases} (V \times V \times V)(x, y, z), \text{ if } kx + my + nz = r, k, m, n \neq 0 \\ V(x), & \text{if } kx = r, k \neq 0, m, n = 0 \\ V(y), & \text{if } my = t, m \neq 0, k, m = 0 \\ V(z), & \text{if } nz = t, n \neq 0, k, m = 0 \\ \sup_{x \in X} V(s) & \text{if } kx + my + nz = t, k, m, n = 0 \\ (0,1) & \text{if } kx + my + nz \neq T \end{cases}$$

for  $x, y, z \in x, k, m, n \in K$ .

Definition 3.5: A NT  $\tau$  on  $V$  is known as a NTVS if the NPF  $N^\oplus: (V \times V \times V \rightarrow V, \tau \times \tau \times \tau) \rightarrow (V, \tau)$  and  $N^{fcircle}: (K \times V, \tau \times x) \rightarrow (V, \tau)$  are NCF. The pair  $(V, \tau)$  is an NTVS if  $\tau$  is an NT on  $V$ .

Definition 3.6: Weaker NTVS: Assume  $V$  as an NVS over the  $K$ .  $\tau$  as an NT on  $V$  then  $(V, \tau)$  is known as weaker NTVS.

Definition 3.7: Stronger NTVS: Consider  $V$  as an NVS over the Neutrosophic field  $K$ .  $\tau$  as an NT on  $V$  then  $(V, \tau)$  is known as stronger NTVS.

Example: 3.8  $R(I)$  is a weaker NTVS over a field  $Q$  and it is a stronger NTVS over a Neutrosophic field  $Q(I)$ .

Example: 3.9  $R(I)$  is a weaker NTVS over a field  $R$  and it is a stronger NTVS.

Example: 3.10  $M_{m \times n}(I) = \{[a_{ij}]: a_{ij} \in Q\}$  is a weaker NTVS over a  $Q$  and it is a stronger NTVS over a Neutrosophic field  $Q(I)$ .

Theorem 3.11 Each stronger NTVS is a weaker NTVS.

Proof: Assume that  $\tau$  is a topology on  $V$  and  $V(I)$ ,  $V$  is weaker NVS  $V(I)$  is stronger NTVS over a Neutrosophic field  $K(I)$ . Meanwhile  $K \text{subse}q K(I)$  for field  $K$ , it follows that  $(V, \tau)$  is a weaker NTVS.

Theorem 3.12 Each stronger (weaker) NTVS is a topological vector space.

Proof: Assume that  $V(I)$  is a stronger NTVS over a Neutrosophic field  $K(I)$ . Noticeably,  $(V(I), +, \cdot)$  is an abelian group.

Assume  $u = a + bl, v = c + dl \in V(I)$ , and  $\alpha = k + ml, \beta = p + nl \in K(I)$  where  $a, b, c, d \in V$  and  $k, n, m, p \in K$ , then

$$\begin{aligned} 1). a(u + v) &= (k + ml)(a + bl + c + dl) \\ &= ka + kc + [kb + kd + ma + mb + mc + md]I \\ &= (k + ml)(a + bl) + (k + ml)(c + dl) \\ &= au + av. \end{aligned}$$

$$\begin{aligned} 2). (a + b)u &= (k + ml + p + nl)(a + bl) \\ &= ka + pa + [kb + pb + ma + na + mb + nb]I \\ &= (k + ml)(a + bl) + (p + nl)(a + bl) \\ &= au + bu \end{aligned}$$

$$3). (ab)u = ((k + ml)(p + nl))(a + bl)$$

$$\begin{aligned}
 &= kpa + [kpb + kna + mpa + mna + knb + mpb + mnb]l \\
 &= (k + ml p + nl)(a + bl) \\
 &= a(bu)
 \end{aligned}$$

4. For  $1 + 1 + 0lK(I)$  we have

$$\begin{aligned}
 1u &= (1 + 0l)(a + bl) \\
 &= a(b + 0 + 0)l \\
 &= a + bl.
 \end{aligned}$$

Therefore,  $V(I)$  is a vector space.  $\tau$  is a topology on  $V$  over the field,  $(V, \tau)$  is topological vector space.

Theorem 3.13 A NT  $\tau$  on  $V$  is a NTVS as long as NPF  $(V \times V \times V, \tau \times \tau \times \tau) \rightarrow (V, \tau)$  is NCF.

Proof: Assume  $\tau$  as a NT  $\tau$  on  $V$  and  $k, m, n \in K$ . Meanwhile,  $k \in K$  is the normal element of  $K$  to  $V$ , then the NPF

$N_V^{Lk,m,n}: (V \times V \times V, \tau \times \tau \times \tau) \rightarrow (V, \tau)$  defined by

$$N((x, y, z), t) = \begin{cases} V(x, y, z) & \text{if } x + y + z = r \\ (0,1) & \text{if } x + y + z \neq r \end{cases} \text{ is NCF.}$$

Also, by definition of NT,  $N^\odot: (K \times V, v \times \tau) \rightarrow (V, \tau)$  is NCF.

Then  $N^\odot \circ N_k: (V, \tau) \rightarrow (V, \tau)$  is defined by

$$N^\odot \circ N_k(x, y) = \begin{cases} V(x) & \text{if } y = kx, k \neq 0 \\ \sup_{s \in X} V(s) & \text{if } y = kx, k = 0 \\ (0,1) & \text{otherwise} \end{cases} \text{ is NCF.}$$

Similarly,  $N^\odot \circ N_m: (V, \tau) \rightarrow (V, \tau)$  defined by

$$N^\odot \circ N_m(z, t) = \begin{cases} V(x) & \text{if } t = mx, m \neq 0 \\ \sup_{s \in X} V(s) & \text{if } y = mz, k = 0 \\ (0,1) & \text{otherwise} \end{cases} \text{ is NCF.}$$

$(N^\odot \circ N_k) \times (N^\odot \circ N_m): (V \times V \times V, \tau \times \tau \times \tau) \rightarrow (V \times V \times V, \tau \times \tau \times \tau)$  described as follows

$$(N^\odot \circ N_k) \times (N^\odot \circ N_m)((x, z), (y, t)) = \begin{cases} (V \times V)(x, z) & \text{if } (x, z) = (y, t) \\ (0,1) & \text{if } (x, z) \neq (y, t) \end{cases}$$

is NCF. Thus,  $N^\oplus \circ [(N^\odot \circ N_k) \times (N^\odot \circ N_m)] = N_V^{Lk,m,n}$  is NCF. On the other hand, Assume  $N_V^{Lk,m,n}$  is NCF for  $k, n, m \in K$ .

Assume the projection mapping  $p_I: (K \times V, v \times \tau) \rightarrow (V, \tau)$  defined as follows:

$$p_I((k, x), z) = \begin{cases} (K \times V)(k, x) & \text{if } z = x \\ (0,1) & \text{otherwise} \end{cases} \text{ and } \theta \text{ is normal of } V, \text{ then } N_\theta: (V, \tau) \rightarrow (V \times V \times V, \tau \times \tau \times \tau) \text{ defined by}$$

$$N_\theta(x, (x_1, y_1)) = \begin{cases} V(x) & \text{if } (x_1, y_1) = (x, \theta) \\ (0,1) & \text{if } (x_1, y_1) \neq (x, \theta) \end{cases}$$

are NCF.

$N_\theta \circ p_I: (K \times V, v \times \tau) \rightarrow (V, \tau)$  is described as follows

$$N_\theta \circ p_I((k_t x)_t (x_{12} y_1)) = \begin{cases} (K \times V)(k_t x) & \text{if } (x_{1t} y_1) = (x, \theta) \\ (0_t 1) & \text{if } (x_{1t} y_1) \neq (x, \theta) \end{cases} \text{ is NCF. Thus } N^\odot = (N_V^{Lk,m,n} \circ N_\theta \circ p_I): (K \times V, v \times \tau) \rightarrow (V, \tau)_t \text{ where}$$

$(N_V^{Lk,m,n} \circ N_\theta \circ p_I)((k, x), z) = \begin{cases} (K \times V)(k, x) & \text{if } z = kx, k \neq 0 \\ \sup_{s \in X} V(s) & \text{if } z = kx, k = 0 \\ (0,1) & \text{if } z \neq kx \end{cases}$  is NCF. Meanwhile  $N_V^{Lk,m,n}$  is NCF for  $k, m \in K$ , taking  $k = 1, m = 1$ . We have

$N^\oplus: (V \times V \times V \rightarrow V, \tau \times \tau \times \tau) \rightarrow (V, \tau)$  is NCF. Therefore, it is proved.

Theorem 3.13:

Definition 3.13: A NPF  $N: V \rightarrow W$  is a neutrosophic linear conversion if

If  $N(\theta, \theta', \theta'') = \sup_{(x,y,z) \in (X \times Y \times Z)} N(x, y, z)$ ,

$$N(kx, ky, kz) = \begin{cases} N(x, y, z) & \text{if } k \neq 0 \\ \sup_{(x,y,z) \in (X \times Y \times Z)} N(x, y, z) & \text{if } k = 0 \end{cases}$$

If  $N(kx, ky, kz) = V(x)$  and  $N(ma, mb, mc) = V(x)$  imply

$N(kx, ky, kz) + N(ma, mb, mc) = V(kx + mz)$  for  $a, x \in X, b, y \in Y, c, z \in Z$  and  $k, m \in K$ .

Theorem 3.14: Assume  $N(X)$  as an NS in vector space over  $X$ . Then

$N(X)$  is an NVS over  $X$ .

For scalar  $\alpha, \beta$  then  $\alpha x + \beta x \subseteq N(X) \forall x \in N(X)$

For scalar  $\alpha, \beta$  and for  $x, y \in N(X)$ , then  $\mu_N(\alpha x + \beta y) \geq \mu_N(x) \wedge \mu_N(y)$ ,  $v_N(\alpha x + \beta y) \leq v_N(x) \vee v_N(y)$  and  $\sigma(\alpha x + \beta y) \leq \sigma_N(x) + \sigma_N(y)$

Proof: Obviously (1)  $\Rightarrow$  (2) and (2)  $\Rightarrow$  (3) by the definition of NVS.

To prove (2)  $\Rightarrow$  (1) :  $N(X) + N(x) = 1. N(X) + 1. N(x) \subseteq N$

$\alpha N(X) = \alpha N(X) + 0N(X) \subseteq N(X)$  This proves the condition.

#### 4. Result Analysis and Discussion

In this part, the performance validation result of the DRDG-NSTVS technique using the DR dataset. The dataset includes 1744 images with five classes labels as showed in Table 1.

Table 1: Details on Dataset

Classes	No. of Images
NoDR (Grade 0)	1017
MildNPDR (Grade 1)	270
Moderate NPDR (Grade 2)	347
Severe NPDR (Grade 3)	75
PDR (Grade 4)	35
Total Images	1744

The DR detection results of the DRDG-NSTVS technique are inspected in Table 2 and Fig. 3. The outcomes performed that the DRDG-NSTVS model gets enhanced recognition results under 5 classes. With 70%TRAS, the DRDG-NSTVS technique provides average  $accu_y$ ,  $prec_n$ ,  $sens_y$ ,  $spec_y$ , and  $F_{score}$  of 98.30%, 91.14%, 78.72%, 98.58%, and 82.83%, respectively. Besides, with 30%TESS, the DRDG-NSTVS model delivers average  $accu_y$ ,  $prec_n$ ,  $sens_y$ ,  $spec_y$ , and  $F_{score}$  of 98.09%, 95.23%, 83.94%, 98.10%, and 88.45%, correspondingly.

Table 2: DR detection outcome of DRDG-NSTVS technique on 70%TRAS and 30%TESS

Class labels	$Accu_y$	$Prec_n$	$Sens_y$	$Spec_y$	$F_{Score}$
TRAS (70%)					
NoDR	97.54	97.08	98.73	95.91	97.90
Mild NPDR	98.93	96.91	96.41	99.41	96.66
Moderate NPDR	98.44	93.10	99.59	98.16	96.24

Severe NPDR	98.03	85.29	60.42	99.57	70.73
PDR	98.52	83.33	38.46	99.83	52.63
Average	98.30	91.14	78.72	98.58	82.83
TESS (30%)					
NoDR	95.80	95.00	98.06	92.52	96.51
Mild NPDR	98.09	94.52	92.00	99.11	93.24
Moderate NPDR	99.43	97.17	100.00	99.29	98.56
Severe NPDR	97.71	89.47	62.96	99.60	73.91
PDR	99.43	100.00	66.67	100.00	80.00
Average	98.09	95.23	83.94	98.10	88.45

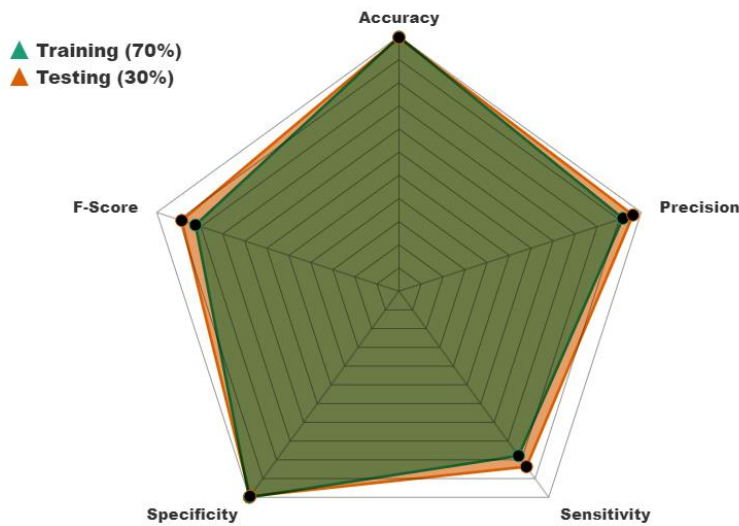


Figure 3: Average outcome of DRDG-NSTVS technique on 70%TRAS and 30%TESS

Inspecting the precision-recall (PR) curve, as presented in Fig. 4, the analysis certified that the DRDG-NSTVS technique increasingly achieves enhanced PR values below every classes. It confirms the upgraded skills of the DRDG-NSTVS system in the classification of diverse class labels, presenting the ability the recognize classes.

Likewise, in Fig. 5, ROC curves created by the DRDG-NSTVS system outdid the identification of dissimilar labels. It offers a complete understanding of the trade-off amongst TPR and FRP over discrete detection values of threshold and epoch counts. The outcome underlined the superior classifier results of the DRDG-NSTVS technique below every class, outlining the efficacy in addressing several classification problems.

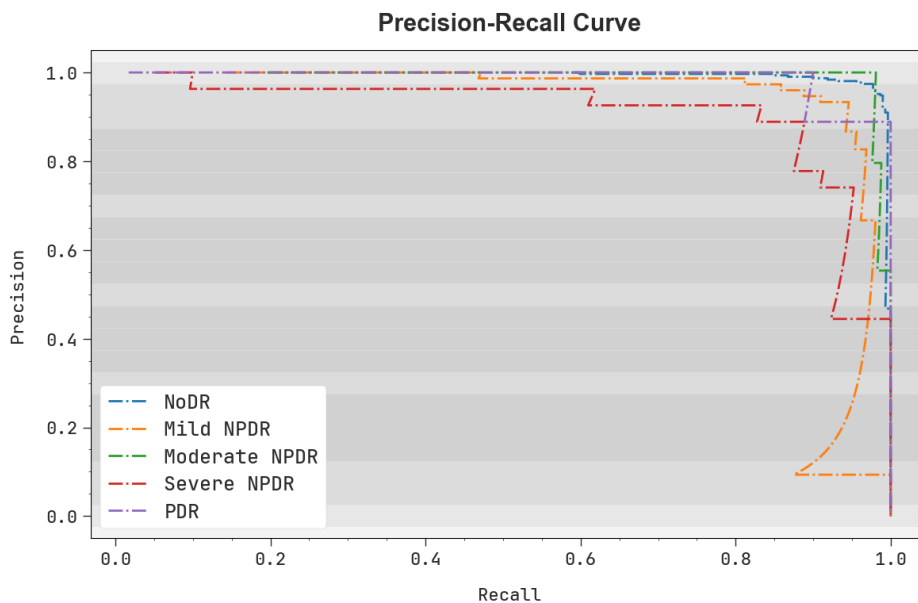


Figure 4: PR curve of the DRDG-NSTVS technique

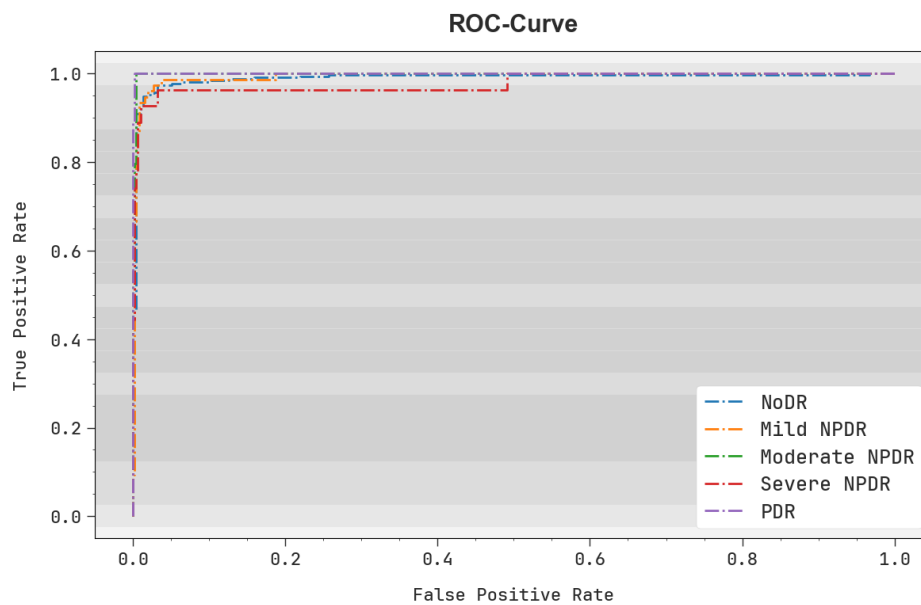


Figure 5: ROC curve of the DRDG-NSTVS technique

In Table 3, a complete comparison study of the DRDG-NSTVS method with recent techniques is given [17, 26].

Fig. 6 demonstrates the  $accu_y$  and  $prec_n$  result of the DRDG-NSTVS method. The experimental results implied the enhanced efficiency of the DRDG-NSTVS approach. Based on  $accu_y$ , the DRDG-NSTVS system gets increased  $accu_y$  of 98.30% while the RBFN Network, KNN, UNet, and CNN with SVM, CNN, DCNN+SVMGA, SVM-GA, and LRDL-WDRI approaches get reduced  $accu_y$  of 93.25%, 95.05%, 94.94%, 95.79%, 97.38%, 96.78%, and 94.45%, correspondingly.

Table 3: Comparative analysis of DRDG-NSTVS technique with recent approaches

Models	$Accu_y$	$Prec_n$	$Sens_y$	$Spec_y$
RBFN Network	93.25	83.56	74.76	93.00
KNN Classifier	95.05	88.15	75.54	92.30
UNet and CNN with SVM	94.94	88.19	74.10	98.08
CNN Algorithm	95.79	85.88	73.76	93.49
DCNN+SVMGA	97.38	85.01	67.18	94.32
SVM-Genetic Algorithm	96.78	81.36	64.66	95.73
LRDL-WDRI	94.45	86.53	69.27	96.32
DRDG-NSTVS	98.30	91.14	78.72	98.58

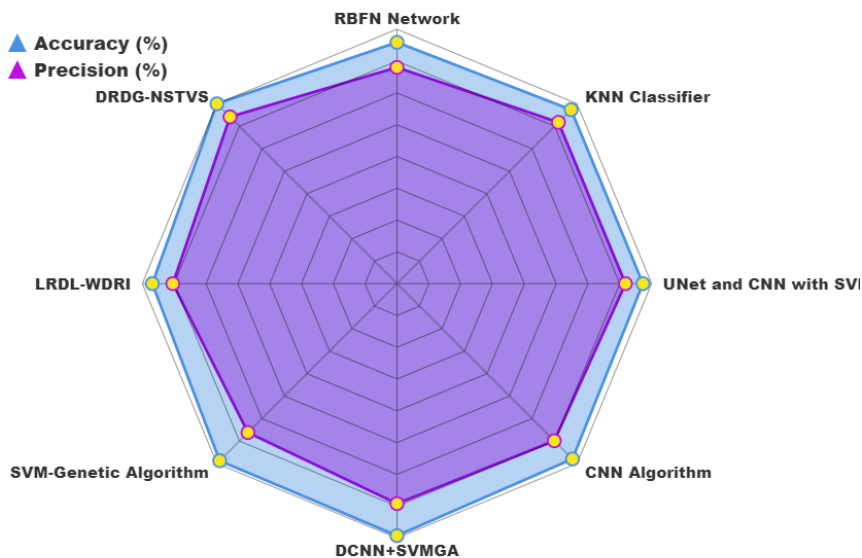


Figure 6:  $Accu_y$  and  $prec_n$  analysis of DRDG-NSTVS technique with recent approaches

Also, based on  $prec_n$ , the DRDG-NSTVS model gains enlarged  $prec_n$  of 91.14% where the RBFN Network, KNN, UNet and CNN with SVM, CNN, DCNN+SVMGA, SVM-GA, and LRDL-WDRI methodologies obtain decreased  $prec_n$  of 83.56%, 88.15%, 88.19%, 85.88%, 85.01%, 81.36%, and 86.53%, correspondingly.

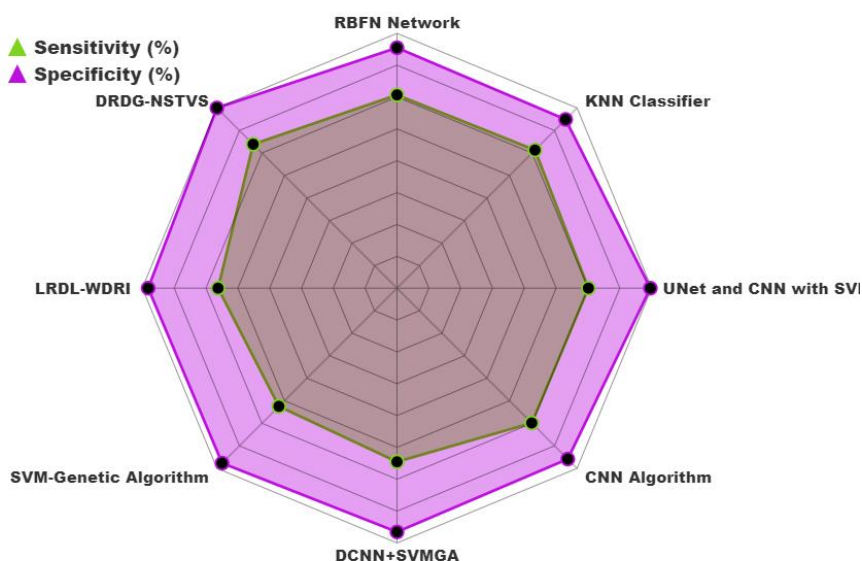


Figure 7:  $Sens_y$  and  $spec_y$  analysis of DRDG-NSTVS technique with recent approaches

Fig. 7 explains the  $sens_y$  and  $spec_y$  outcome of the DRDG-NSTVS method. The experimental results implied the improved efficiency of the DRDG-NSTVS model. Based on  $sens_y$ , the DRDG-NSTVS system gains improved  $sens_y$  of 78.72% but the RBFN Network, KNN, UNet and CNN with SVM, CNN, DCNN+SVMGA, SVM-GA, and LRDL-WDRI methodologies get decreased  $sens_y$  of 74.76%, 75.54%, 74.10%, 73.76%, 67.18%, 64.66%, and 69.27%, correspondingly. Similarly, based on  $spec_y$ , the DRDG-NSTVS approach gains improved  $spec_y$  of 98.58% whereas the RBFN Network, KNN, UNet and CNN with SVM, CNN, DCNN+SVMGA, SVM-GA, and LRDL-WDRI techniques obtain decreased  $spec_y$  of 93.00%, 92.30%, 98.08%, 93.49%, 94.32%, 95.73%, and 96.32%, correspondingly.

## 5. Conclusion

In this manuscript, we have proposed a robust DRDG-NSTVS approach on fundus images. It encompasses four different stages involving MF-based preprocessing, feature extraction using InceptionV3, parameter selection using MFO, and NSTVS-based DR classification stages. Initially, the DRDG-NSTVS technique takes place MF noise removal to optimize the clarity of fundus photographs by successfully eliminating noises. Later, the InceptionV3 is used to perform feature extraction for identifying complicated features and patterns related to DR. The parameter tuning is performed by the MFO technique to ensure superior performance of the model. The final diagnoses and classification of DR are accomplished using the NSTVS classifiers that easily perform the uncertainties inherent in medicinal statistics. The simulation was conducted on a benchmark dataset to examine the proposed model performance. This combined method gives a greatly reliable and accurate solution for the earlier diagnosis and detection of DR.

**Funding:** “This research received no external funding”

**Conflicts of Interest:** “The authors declare no conflict of interest.”

## References

- [1] Dhanalakshmi, G., Sandhiya, S. and Smarandache, F., 2024. Selection of the best process for desalination under a Treesoft set environment using the multi-criteria decision-making method. *International Journal of Neutrosophic Science*, 23(3), pp.140-40.
- [2] Almuhur, E., Miqdad, H., Al-labadi, M. and Idrisi, M.I., 2024.  $\mu$ -L-Closed Subsets of Noetherian Generalized Topological Spaces. *International Journal of Neutrosophic Science*, 23(3), pp.148-48.
- [3] Tashtemirovich, A.O., Balba, M.E., Ibrohimjon, F. and Batirova, N., Investigating the Impact of Artificial Intelligence on Digital Marketing Tactics Strategies Using Neutrosophic Set.
- [4] Sivakumar, C., Al-Qadri, M.O., Alsaraireh, A.A., Al-Husban, A., Meenakshi, P.M., Rajesh, N. and Palanikumar, M., 2024. q-rung square root interval-valued neutrosophic sets with respect to aggregated operators using multiple attribute decision making. *International Journal of Neutrosophic Science*, 23(3), pp.154-54.
- [5] Gharib, M., Fakhry, A.E., Ali, A.M., Abdelhafeez, A. and Elbehiery, H., 2024. Single Valued Neutrosophic Sets for Analysis Opinions of Customer in Waste Management. *International Journal of Neutrosophic Science*, 23(3), pp.184-84.
- [6] K. Shankar, Y. Zhang, Y. Liu, L. Wu, and C.-H. Chen, “Hyperparameter tuning deep learning for diabetic retinopathy fundus image classification,” *IEEE Access*, vol. 8, pp. 118164–118173, 2020.
- [7] O. M. Al-Hazaimeh, A. Abu-Ein, N. Tahat, M. Al-Smadi, and M. Al-Nawashi, “Combining artificial intelligence and image processing for diagnosing diabetic retinopathy in retinal fundus images,” *Int. J. Online Biomed. Eng.*, vol. 18, no. 13, pp. 131–151, Oct. 2022.
- [8] W. L. Alyoubi, M. F. Abulkhair, and W. M. Shalash, “Diabetic retinopathy fundus image classification and lesions localization system using deep learning,” *Sensors*, vol. 21, no. 11, p. 3704, May 2021.
- [9] N. Gharaibeh, O. M. Al-Hazaimeh, B. Al-Naami, and K. M. Nahar, “An effective image processing method for detection of diabetic retinopathy diseases from retinal fundus images,” *Int. J. Signal Imag. Syst. Eng.*, vol. 11, pp. 206–216, Jan. 2018.
- [10] K. Shankar, A. R. W. Sait, D. Gupta, S. K. Lakshmanprabu, A. Khanna, and H. M. Pandey, “Automated detection and classification of fundus diabetic retinopathy images using synergic deep learning model,” *Pattern Recognit. Lett.*, vol. 133, pp. 210–216, May 2020.
- [11] Albelaihi, A. and Ibrahim, D.M., 2024. DeepDiabetic: An Identification System of Diabetic Eye Diseases Using Deep Neural Networks. *IEEE Access*.
- [12] Ibrahim, D.M., Elshennawy, N.M. and Sarhan, A.M., 2021. Deep-chest: Multi-classification deep learning model for diagnosing COVID-19, pneumonia, and lung cancer chest diseases. *Computers in biology and medicine*, 132, p.104348.
- [13] Albahli, S. and Nazir, T., 2023. A Circular Box-Based Deep Learning Model for the Identification of Signet Ring Cells from Histopathological Images. *Bioengineering*, 10(10), p.1147.
- [14] Alhasson, H.F., Almozainy, E., Alharbi, M., Almansour, N., Alharbi, S.S. and Khan, R.U., 2023. A Deep Learning-Based Mobile Application for Monkeypox Detection. *Applied Sciences*, 13(23), p.12589.

- [15] Wirtz, A., Mirashi, S.G. and Wesarg, S., 2018. Automatic teeth segmentation in panoramic X-ray images using a coupled shape model in combination with a neural network. In *Medical Image Computing and Computer Assisted Intervention–MICCAI 2018: 21st International Conference, Granada, Spain, September 16-20, 2018, Proceedings, Part IV 11* (pp. 712-719). Springer International Publishing.
- [16] Hai, Z., Zou, B., Xiao, X., Peng, Q., Yan, J., Zhang, W. and Yue, K., 2024. A novel approach for intelligent diagnosis and grading of diabetic retinopathy. *Computers in Biology and Medicine*, 172, p.108246.
- [17] Raiaan, M.A.K., Fatema, K., Khan, I.U., Azam, S., Rashid, M.R.U., Mukta, M.S.H., Jonkman, M. and De Boer, F., 2023. A lightweight robust deep learning model gained high accuracy in classifying a wide range of diabetic retinopathy images. *IEEE Access*, 11, pp.42361-42388.
- [18] Romero-Oraá, R., Herrero-Tudela, M., López, M.I., Hornero, R. and García, M., 2024. Attention-based deep learning framework for automatic fundus image processing to aid in diabetic retinopathy grading. *Computer Methods and Programs in Biomedicine*, 249, p.108160.
- [19] Yamin, M., Basahel, S., Bajaba, S., Abusurrah, M. and Lydia, E.L., 2023. Leveraging Retinal Fundus Images with Deep Learning for Diabetic Retinopathy Grading and Classification. *Computer Systems Science & Engineering*, 46(2).
- [20] Shamrat, F.J.M., Shakil, R., Akter, B., Ahmed, M.Z., Ahmed, K., Bui, F.M. and Moni, M.A., 2024. An advanced deep neural network for fundus image analysis and enhancing diabetic retinopathy detection. *Healthcare Analytics*, 5, p.100303.
- [21] Chavan, S. and Choubey, N., 2023. An automated diabetic retinopathy of severity grade classification using transfer learning and fine-tuning for fundus images. *Multimedia Tools and Applications*, 82(24), pp.36859-36884.
- [22] Jana, B.R., Thotakura, H., Baliyan, A., Sankararao, M., Deshmukh, R.G. and Karanam, S.R., 2023. Pixel density based trimmed median filter for removal of noise from surface image. *Applied Nanoscience*, 13(2), pp.1017-1028.
- [23] Meena, G., Mohbey, K.K. and Kumar, S., 2023. Sentiment analysis on images using convolutional neural networks based Inception-V3 transfer learning approach. *International journal of information management data insights*, 3(1), p.100174.
- [24] Fan, Q., Ma, Y., Wang, P. and Bai, F., 2024. Otsu Image Segmentation Based on a Fractional Order Moth–Flame Optimization Algorithm. *Fractal and Fractional*, 8(2), p.87.
- [25] Kungumaraj, E., Lathanayagam, E., Saikia, U., Anand, M.C.J., Khanna, S.T., Martin, N., Tiwari, M. and Edalatpanah, S.A., 2023. Neutrosophic Topological Vector Spaces and its Properties. *International Journal of Neutrosophic Science*, 23(2), pp.63-3.
- [26] Jena, P.K., Khuntia, B., Palai, C., Nayak, M., Mishra, T.K. and Mohanty, S.N., 2023. A novel approach for diabetic retinopathy screening using asymmetric deep learning features. *Big Data and Cognitive Computing*, 7(1), p.25.